ELSEVIER

Journal of Power Sources 94 (2001) 51–62

JOURNAL OF POWER SOURCES

www.elsevier.com/locate/jpowsour

Experimental study on the dynamic characteristics of kW-scale molten carbonate fuel cell systems

Byoung Sam Kang*, Joon-Ho Koh, Hee Chun Lim

Korea Electric Power Research Institute, 103-16 Munji-dong, Yusong-ku, Taejon 305-380, South Korea

Received 8 August 2000; accepted 5 October 2000

Abstract

The aim of this work is to develop dynamic models for two types of kW-scale molten carbonate fuel cell (MCFC) systems on the basis of experimental data. The dynamic models are represented as a 3×3 transfer function matrix for a multi-input and multi-output (MIMO) system with three inputs and three outputs. The three controlled variables which severely affect the stack performance and lifetime are the temperature difference in the stack and the pressure drop at the anode and the cathode. Three manipulated variables, namely, current load, fuel and oxidant utilization, are selected to keep the three controlled variables within their safety limits for the reliable operation and protection of the system in case of emergency. Each element in the transfer function matrix is in the form of a first-order model using a simple, unit step, response test during operation. The non-zero off-diagonal elements in the transfer function matrix show that some interactions exist among the operating variables, and two zeros show no interaction between fuel and oxidant flow without gas cross-over. The stability of both dynamic models is analyzed using the relative gain array (RGA) method. Large diagonal elements in the RGA matrix show that the pairing between the manipulated and controlled variables is appropriate. Proper pairing is also proven by the singular value analysis (SVA) method with a smaller singular value in each system.

Keywords: MCFC; MIMO; Dynamic model; Transfer function; Step response

1. Introduction

The molten carbonate fuel cell (MCFC) power generating system has several advantages, e.g. high efficiency and co-generation capability, over low-temperature fuel cells because of its high operating temperature (650°C) [1]. MW-class MCFC power systems have prospects to become one of the major electric power plants of the future [2,3]. To reach the commercialization stage, however, some problems still have to be solved to improve the performance of the MCFC system. Unlike other types of fuel cell, the vulnerability of molten electrolyte to abrupt pressure change and the differential expansion of each component due to the high temperature difference in the stack cause major problems. The pressure difference between the anode and the cathode above the safety limit damages the cells by causing gas cross-over and hot spots in the stack [4]. A temperature difference of several hundred degrees in the stack at the maximum current load can cause corrosion, material degradation, and electrolyte loss [5,13]. Such parameters are critical factors for stable performance and they should be carefully controlled within the safety limit for reliable operation with a high overall system efficiency.

In most recent studies controlled variable is the power output to follow the demand of electric load from customers, while the manipulated variables are current load, fuel, and air flow. Dynamic models have been developed [7–9] to understand the transient behavior of fuel-cell systems in load following. Some simulation results have been reported [10,11,14] for system faults and plant trip. These two control strategies are referred to as 'servo' and 'regulator' control [12]. The performance decay of MCFC stacks during operation makes it more preferable to operate the system with a constant optimal current load rather than through tracking the various electric load demands of customers. The excess power generated in the system can be used in sub-systems, such as the fuel processor and parasitic power. In this study, the controlled variables selected are the temperature difference in the stack and the anode and cathode pressure drop. These variables should be controlled to protect the system from damage in the case of emergencies, such as system shut down and trip.

The important parameters which affect the controlled variables include: fuel and oxidant flow, operating pressure, stack inlet temperature, current load, cell size, cell number,

* Corresponding author. Tel.: +82-42-865-5397; fax: +82-42-865-5374.
E-mail address: bskang@kepri.re.kr (B.S. Kang).

0378-7753/01/$ – see front matter
PII: S0378-7753(00)00606-6

Nomenclature

dT	temperature difference in the stack (°C)
dP	pressure drop in the stack
g_{ji}	transfer function between u_i and y_j
G	overall transfer function matrix with nine elements
i	current density (mA cm^{-2})
I	current load (A)
K	steady-state gain matrix
K_{ji}	steady-state gain ($i = 1, 2, 3, j = 1, 2, 3$)
u_i	manipulated variable ($i = 1, 2, 3$)
U	input vector with three elements
U_f	fuel utilization in anode
U_{ox}	oxygen utilization in cathode
y_j	controlled variable ($j = 1, 2, 3$)
Y	output vector with three elements

Greek letters

θ	time delay (s)
τ	time constant (s)
λ_{ji}	relative gain ($i = 1, 2, 3, j = 1, 2, 3$)
Λ	relative gain array

Subscripts

a	anode side
c	cathode side
in	stack inlet
out	stack outlet

Superscript

T	transpose

external heaters. Among these parameters, the electrical load and the fuel and oxidant utilization were chosen as the manipulated variables, as these influence the controlled variables more than the others [15]. The dynamic model of the MCFC system in this study can be represented as a transfer function matrix, which shows the dynamic relation between three controlled and three manipulated variables in a Laplace transform [12]. The multi-input and multi-output (MIMO) system, an MCFC power generating system, has interaction among the operating variables used in the fuel cell stack or other sub-systems, such as the fuel processor, the inverter, and the heat recovery unit [7–11]. A stronger interaction will occur in a fuel cell stack with an internal reforming stack than in one with an external reform. Our study aims at establishing a dynamic model for MCFC systems with external reformers which can possibly use synthetic fuel from coal gas as well as reformed natural gas. The dynamic models used in most of the past studies have been confined to simulation models, based on physical laws. Modeling uncertainties and constantly changing operating conditions make it very difficult, however, to develop reliable dynamic models for MCFC systems.

In this paper, we develop dynamic models for of two types of kW-scale MCFC systems on the basis of experimental data. These dynamic models, represented as 3×3 transfer function matrix, are derived from the response for a unit step-change of the manipulated variables. Discussion is also included of the stability of the dynamic models using the relative gain array (RGA) and the singular value analysis (SVA) methods. These dynamic models, can be used as one component in simulating the overall MCFC system, which is composed of a fuel processor, a fuel cell, a power unit conversion, heat and a recovery unit [8]. The dynamic characteristics at atmospheric operation can be applied to pressurized operation with different base pressures [6].

2. Dynamic models of MIMO systems and stability analysis

2.1. Dynamic models of MIMO systems

The stack considered for this study is composed of repeating planar unit cells and co-flow type internal gas manifolds. Fig. 1 shows the schematic view of a co-flow MCFC stack with upper and lower heating plates used for heating the stack at constant temperature (650°C). Each repeating element, i.e. unit cell, is made up of an anode, a cathode, electrolyte melt in a matrix, and a separator which is used for electrical interconnection between unit cells and separation of each electrode gas. The cell in the stack produces electricity by the electrochemical reaction of fuel and oxidant. The following reactions take place in electrodes under external current load.

$$H_2 + {CO_3}^{2-} \rightarrow H_2O + CO_2 + 2e^- \quad \text{(anode)} \tag{1}$$

$$CO_2 + \tfrac{1}{2}O_2 + 2e^- \rightarrow {CO_3}^{2-} \quad \text{(cathode)} \tag{2}$$

The overall reaction is exothermic because of a negative enthalpy change and the incomplete conversion from fuel to electricity.

$$H_2 + \tfrac{1}{2}O_2 \rightarrow H_2O + \text{electricity} + \text{heat} \quad \text{(overall)} \tag{3}$$

In the case of a co-flow stack under load, the temperature of a given separator tends to increase with gas flow due to the exothermic electrochemical reaction. As a result, the inlet-side has the lowest temperature and the outlet-side the highest. The large temperature difference in the stack causes thermal stress of the components and accelerates high-temperature corrosion of the materials [4]. To lower this temperature difference in the stack, cathode gas is recycled with pressurized operation to provide cooling. The details of such an a procedure have been reported elsewhere [16]. Even though increase of oxidant flow is an effective way to control the temperature difference, the excess amount of compressed air is limited to maintain the pressure difference between anode and cathode. Since the components of the stack are very vulnerable to breakage by abrupt pressure

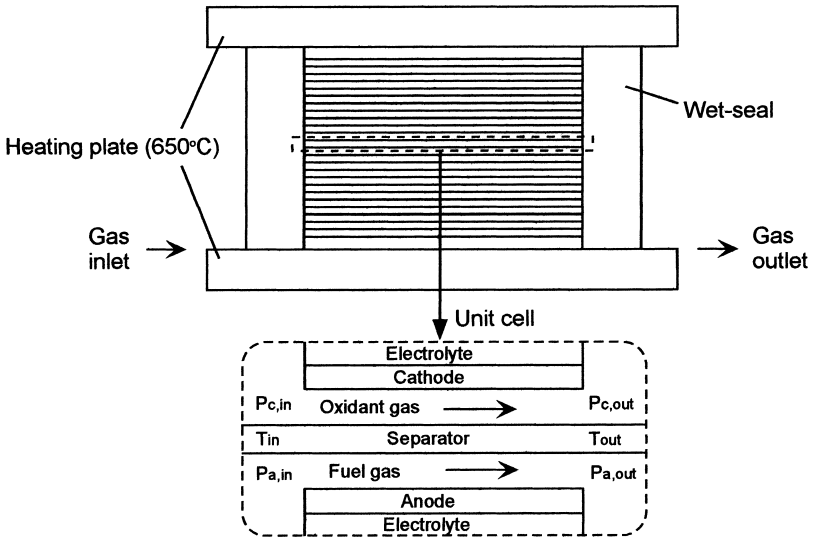

Fig. 1. Schematic of a co-flow MCFC stack and its unit cell structure including controlled variables.

change in an emergency situation, the pressure difference should be maintained within the safety limit before purging with nitrogen. The pressure difference limit between anode and cathode over the specified range (200 mm H_2O) is highly detrimental to the stack performance by causing gas cross over and hot spots in the stack. In order to operate the MCFC system with stable performance and high overall system efficiency, the controlled variables should be the temperature difference in the stack and the pressure drop at the anode and the cathode. The three controlled variables in the stack are shown in Fig. 1. The gas pressure is measured by the difference between the pressure in the stack and atmospheric pressure using water filled manometers. The pressure difference between the anode and the cathode can be calculated from the measured pressure for each.

The control variables and their specific operating conditions are listed in Table 1. The order of the controlled variables is determined according to their manipulated variables. The maximum temperature (680°C) in the stack can be used as the limit of the controlled variable instead of the temperature difference, because the inlet temperature is fixed at 580°C. The stack inlet temperature, the anode and the cathode outlet pressures are chosen as the disturbance variables, which should be kept constant without unmeasured disturbances. All the variables in Table 1 are used in a normalized deviation form [12]. The steady-state operating conditions of kW-scale stacks are considered to be a current density of 100 mA/cm^2 and 40% utilization of fuel and oxidant. The relationship between the input and output (manipulated and controlled) variables can be represented as a transfer function $g_{ji}(s)$ between inputs u_i and outputs y_j $(i, j = 1, 2, 3)$ (Fig. 2), i.e.

$$\frac{y_j}{u_i} = g_{ji}(s) \tag{4}$$

Each transfer function can be represented by a first-order plus time delay model as in Fig. 3, i.e.

$$g_{ji}(s) = \frac{K_{ji}}{\tau_{ji}s + 1} \exp(-\theta_{ji}s) \tag{5}$$

where K_{ji} is the static gain, τ_{ji} a time constant, θ_{ji} the time delay. Fig. 3 shows that the response of the first-order

Table 1
Specification of control variables in large cell area MCFC stacks

Control variables	Item	Specification
Manipulated variable (MV)	i (current density) (mA cm^{-2})	0∼150
	U_f (fuel utilization) (%)	40∼80
	U_{ox} (oxidant utilization) (%)	30∼60
Controlled variable (CV)	dT ($T_{out} - T_{in}$) (°C)	≤100
	dP_a ($P_{a,in} - P_{a,out}$) (mm H_2O)	≤200
	dP_c ($P_{c,in} - P_{c,out}$) (mm H_2O)	≤200
Disturbance variable (DV)	T_{in} (stack inlet temperature) (°C)	580
	$P_{a,out}$ (anode outlet pressure) (atm)	1
	$P_{c,out}$ (cathode outlet pressure) (atm)	1

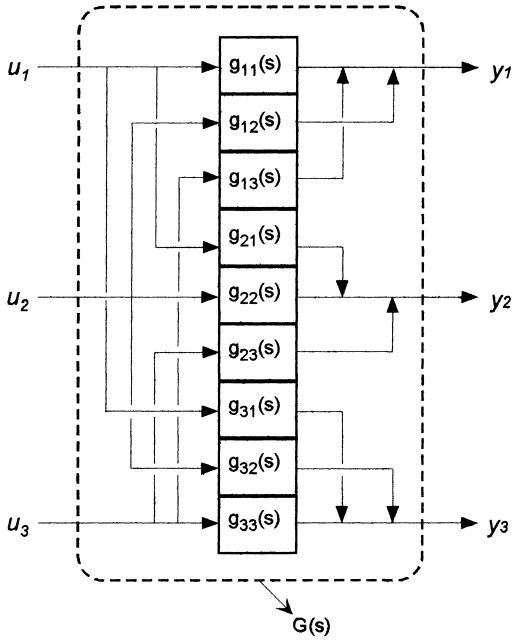

Fig. 2. Multi-input multi-output process (3×3) ($G(s)$: transfer function matrix; g_{ji}: transfer function; u_i: manipulated variable; y_j: controlled variable; $i, j = 1, 2, 3$).

process plus time delay model to the unit step input. After a time interval equal to the process time constant (i.e. for $t = \tau$), the process response reaches 63.2% of its steady-state value. The important parameters in the above system can be easily acquired from graphical interpretation. Several methods for the design of effective control systems to develop empirical dynamic models from the step response model have been explained in detail [12].

If all the $g_{ji}(s)$ are open-loop stable and non-singular, the MIMO process (in this case, 3×3) can be shown as the overall transfer function matrix, $G(s)$, as shown in Fig. 2. These input–output relationships can be expressed in the vector-matrix notation as

$$Y(s) = G(s)U(s) \tag{6}$$

where $Y(s)$ and $U(s)$ are vectors with three elements, namely,

$$Y(s) = \begin{bmatrix} y_1(s) \\ y_2(s) \\ y_3(s) \end{bmatrix}, \qquad U(s) = \begin{bmatrix} u_1(s) \\ u_2(s) \\ u_3(s) \end{bmatrix} \tag{7}$$

and $G(s)$ is the process transfer function matrix

$$G(s) = \begin{bmatrix} g_{11}(s) & g_{12}(s) & g_{13}(s) \\ g_{21}(s) & g_{22}(s) & g_{23}(s) \\ g_{31}(s) & g_{32}(s) & g_{33}(s) \end{bmatrix} \tag{8}$$

In the above case, the process transfer function matrix is composed of nine transfer functions. If the $g_{ji}(s)$:$(j \neq i)$ are non-zero transfer functions, there are interactions between the controlled variables and the manipulated variables; that is, each manipulated variable can affect one or another of the controlled variables. These interactions make it difficult to control the process system and operate it with reliability. The zero off-diagonal elements show no interaction between the relative operating variables.

The step response test used to determine first-order or over-damped systems is a quick means for achieving some reasonable designs without too much computational effort, although some fine-tuning may have to be executed subsequently to obtain more acceptable responses [20]. Fig. 3 shows a typical step response model of first-order plus time delay. This information is sufficient to construct a simple first-order plus time delay model and it is also desirable to seek dynamic interaction measures which are merely based on such information. If the dynamic characteristics are negligible ($\tau \approx 0$) and so is time delay ($\theta \approx 0$), the dynamic transfer function can be reduced to the steady-state gain matrix. The steady-state model can be expressed in terms of deviation variables as follows:

$$y_1 = K_{11}u_1 + K_{12}u_2 + K_{13}u_3 \tag{9}$$

$$y_2 = K_{21}u_1 + K_{22}u_2 + K_{23}u_3 \tag{10}$$

$$y_2 = K_{31}u_1 + K_{32}u_2 + K_{33}u_3 \tag{11}$$

where K_{ji} denotes the steady-state gain between y_j and u_i

$$K_{ji} = \left(\frac{\partial y_j}{\partial u_i}\right)_u \tag{12}$$

and $(\partial y_j/\partial u_i)_u$ denotes a partial derivative which is evaluated with all of the manipulated variables except u_i held constant. The above steady-state model can be expressed more compactly in matrix notation as

$$Y = KU \tag{13}$$

The steady-state model in Eq. (13) is related to the dynamic model in Eq. (6) by

$$K = G(0) = \lim_{s \to 0} G(s) \tag{14}$$

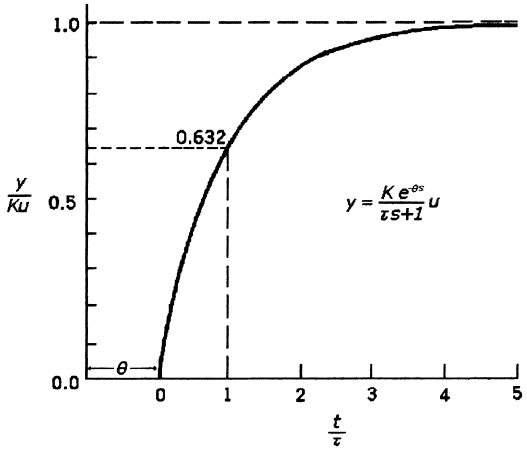

Fig. 3. Unit step response of first-order plus time delay model (y: output; u: input; K: steady-state gain; τ: time constant; θ: time delay).

2.2. Stability analysis of MIMO system based on steady-state gain

Interactions arising in a multi-variable environment produce several undesirable effects for control design. For example, cross coupling between input and output variables prevents the controller from being designed independently and makes the overall process system unstable. The steady-state gain matrix can be used to evaluate a measure of steady-state interactions between controlled and manipulated variables. Consequently, proper pairing of input and output variables to minimize interactions is of paramount importance. To achieve this, the RGA has found widespread acceptance both in industry and in academia and has much more than a simple measure of interactions [17–19]. The relative gain λ_{ji} between the controlled variable y_j and manipulated variable, u_i, is defined by the dimensionless ratio of two steady-state gains, i.e.

$$\lambda_{ji} = \frac{(\partial y_j/\partial u_i)_U}{(\partial y_j/\partial u_i)_Y} \tag{15}$$

and relative gain array, Λ is

$$\Lambda = \begin{bmatrix} \lambda_{11} & \lambda_{12} & \lambda_{13} \\ \lambda_{21} & \lambda_{22} & \lambda_{23} \\ \lambda_{31} & \lambda_{32} & \lambda_{33} \end{bmatrix} \tag{16}$$

The relative gain can be evaluated from the partial derivative with all of the manipulated variables except u_i held constant, as already explained. The relative gain can be also expressed as the dimensionless ratio of open-loop gain to closed loop gain [12]. This method gives a measure of the process interactions and recommends effective pairing between manipulated and controlled variables [17–21].

The SVA can be used to solve the selection of controlled and manipulated variables, and determination of the best multi-loop control configuration. The SVA method is also based on the steady-state gain matrix and singular values, which are non-negative numbers that are defined as the positive square root of the eigen-values of $K^{\mathrm{T}}K$ in Eq. (13). The condition number is defined as the ratio of the largest and smallest non-zero singular value. The condition number is a positive number that provides a measure of the extent to which the gain matrix is ill-conditioned. It also provides useful information on the sensitivity of the matrix properties to variations in the elements of the matrices. The matrix property is related to control system robustness [12]. More advanced methods to solve the interactions between the system variables can be used [20,21], but they are a little beyond the scope of this study.

3. Operation tests of kW-scale MCFC stacks

Two stacks were operated for this study. The specifications of two types of kW-scale MCFC stacks are listed in Table 2. The major differences between the two stacks are electrode area, number of unit cells, and separator type. These differences affect the dynamics of the kW-scale stacks.

The cells were made of Ni–10 wt.%Cr alloy for the anode, NiO for the cathode, 62%Li–38%K carbonate for the electrolyte, and a ceramic matrix (γ-$LiAlO_2$) for the electrolyte support. These are a set of state-of-the-art cell component materials which are widely used at present. The separator size of a 6-kW stack is 600 × 820 mm, and that of a 3-kW stack is 814 × 1200 mm, respectively. Hard-rail type

Table 2
Specification of the 6-kW and 3-kW MCFC stacks

Item	Specification
Performance	
Maximum output power	7.6 kW (6-kW stack) and 3.7 kW (3-kW stack) 16.8 V at 450 A (6-kW stack) and 3.99 V at 900 A (3-kW stack)
Design performance	0.8 V at 150 mA cm^{-2}
Lifetime	5760 h (6-kW stack) and 2230 h (3-kW stack)
Stack configuration	
Effective electrode area	3000 cm^2 (6-kW stack) and 6000 cm (3-kW stack)
No. of unit cells	20 (6-kW stack) and 5 (3-kW stack)
Separator type	Hard rail (6-kW stack) and soft rail (3-kW stack)
Manifold	Internal
Gas distribution	Co-flow
Operating condition	
Pressure	1 atm.
Temperature	650°C
Supplied gases	
Anode	$H_2/CO_2/H_2O$ = 72/18/10, reformed gas
Cathode	$N_2/O_2/CO_2$ = 55/15/30
Utilization	
Anode	40–80
Cathode	30–70

separators, used for the 6-kW stack, were made by etching the gas channels. Soft-rail type separators, used for the 3-kW stack, were made in the form of corrugating center plates which also function as current-collectors. Separators are usually made with SUS 316L steel and coated with aluminium to endure the corrosive conditions imposed by high temperature and the melting matrix. The design pressure drop of the anode gas channel is 20 mm H_2O and that of cathode gas channel is 60 mm H_2O.

The stack was heated from top and bottom by electrical heating plates which, in turn, were electrically separated by mica plates. The outer surface of the stack was thermally insulated. The anode and cathode gases flowed in a co-flow direction and the gas flow pattern inside the stack was a reverse *U*-configuration from the side view. To obtain the temperature profile inside the stack, five thick temperature plates equipped with 12 thermocouples were inserted in the 6-kW stack and three thick plates with fifteen thermocouples were installed in the 3-kW stack.

The feed amounts of fuel and oxidant were determined by the electrical load and gas utilization. Stack performance was measured mostly at 100 and 150 mA cm^{-2} with a fuel utilization rate of 40–80% and an oxidant utilization rate of 30–70%. The inlet gas temperature to the stack was in the range of 500–580°C. Gas pressures were measured with water-filled manometers at the stack inlet and outlet for each gas stream. The detailed operation results of the 6-kW stack were reported in terms of initial performance, voltage distribution, and endurance and decay rate [4].

The unit step change of each manipulated variable to the respective controlled variable was used to acquire the steady-state gain and time constant as a form of performance test during continuous operation. All the data used at the unit step test were recorded in a data-monitoring system at each sampling time.

4. Results and discussion

4.1. Steady-state characteristics of kW-scale MCFC systems

4.1.1. The 6-kW MCFC system

The steady-state gain was evaluated by calculating the relative change of a controlled variable to that of the relevant manipulated variable with the other manipulated variables held constant (Eq. (12)). The operating variables used to calculate the static gain were in a normalized deviation form, which showed the quantity deviated from the steady-state variable divided by the possible operating range. The 6-kW MCFC stack was operated mainly at 100 mA cm^{-2} with $U_f = U_{ox} = 40\%$, which was the steady-state operation condition used in the unit step test.

Fig. 4 shows the effect of current load on the stack inlet and outlet temperatures, which were measured during the operation. The fuel and oxidant flow rates at the open-circuit

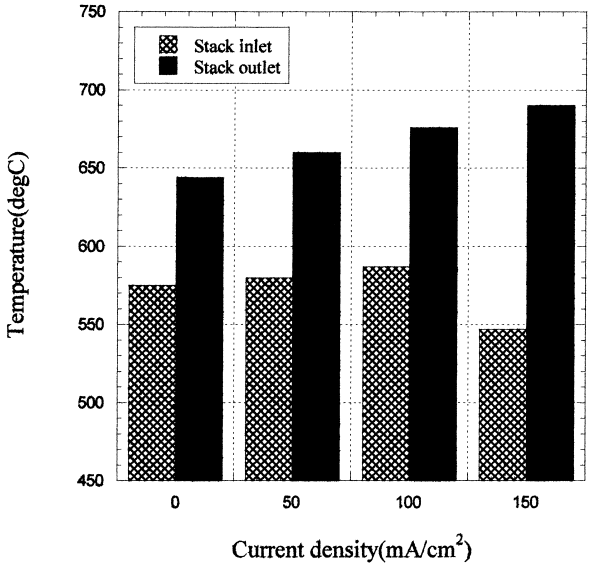

Fig. 4. Effects of current load on temperature at inlet and outlet measured in 6-kW MCFC stack at $U_f/U_{ox} = 40/40\%$.

voltage (OCV) were same as those of the steady-state condition. The difference of stack temperature between the inlet and the outlet increases linearly from OCV to 100 mA cm^{-2}, as shown in Fig. 4. The coldest zone occurred at the middle part of stack inlet due to the upper and lower heating plates and co-flow type gas distribution, as shown in Fig. 1. For this reason, the temperature at the stack inlet was referred to as the minimum temperature in the stack. The outlet temperature was considered to be the maximum temperature, which occurred at the central zone near the outlet due to the exothermic electrochemical reaction (Eq. (3)). As the current density was increased from 0 to 100 mA cm^{-2}, the internal heat produced under load raised the inlet temperature of the stack slightly. From this trend (Fig. 4), it is concluded that there is a linear relationship between maximum temperature and current load. When the load current density was set at 150 mA cm^{-2}, the temperature difference in the stack rose abruptly to 140°C. The stack inlet temperature was lowered to 547°C to keep the stack outlet temperature below 700°C to avoid high-temperature corrosion, as already explained. The lowered inlet temperature (about 34°C) was considered as the measured disturbance to the stack inlet temperature. The other way to operate this stack with the higher load current density, 150 mA cm^{-2}, at atmospheric pressure is to lower oxidant utilization <20% [15]. Such a low oxidant utilization should be avoided, however, to maintain the pressure difference in the stack within the allowable range. To solve this thermal management in the external reforming stack configuration, pressurized operation should be considered to increase the flow of coolant air without increasing the pressure difference in the stack [16].

The pressure drop in the stack was mostly created in the narrow gas channels and decreased with current load. Fig. 5 shows the effect of current load on the pressure at the anode

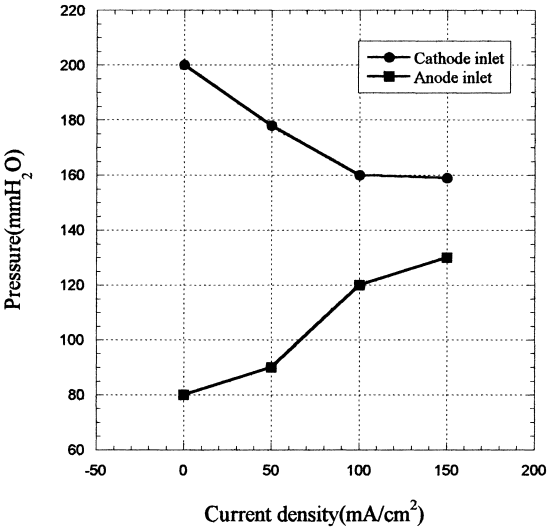

Fig. 5. Effects of current load on anode and cathode inlet pressure measured in 6-kW MCFC stack at $U_f/U_{ox} = 40/40\%$.

and the cathode inlets, assuming the anode and cathode outlet pressures to be zero. The measured pressure difference between anode and cathode decreases gradually from OCV to 150 mA cm^{-2}, since the cathode reaction consumes 1.5 mol of reactant gases while the anode produces 2 mol of gases (Eqs. (1) and (2)) under load operation. This trend is contrary to the effect on the temperature difference in the stack, as shown in Fig. 4. The two opposing trends also show that the optimal operating conditions for a given stack should be considered. The pressure of the cathode inlet is higher than that of the anode at the same utilization, since the volumetric flow of cathode gas is much higher than that of anode gas by using air including inert nitrogen as the oxidant gas. The almost same pressure at the cathode inlet at different current densities, namely, 100 and 150 mA cm^{-2}, indicates that the pressure difference cannot be lowered any more at a fixed fuel and oxidant utilization (40%).

The effects of fuel and oxidant utilization on the pressure drops are given in Table 3, which are measured by changing the gas flow during the operation. The pressure drops at the anode and the cathode appear to be inversely proportional to the utilization rate, which shows a negative static gain in the steady-state gain matrix (Eq. (17)). The outlet gas dynamic pressure was set to atmosphere in terms of absolute pressure to account for only the net pressure drop across the gas channels, as shown in Table 3. The measured gas dynamic pressure at the stack outlet was, in fact, a little higher than zero because of the flow resistance in the exhaust line (mostly from pipes and valves), which was also considered to be a disturbance variable. The pressure drop at each electrode was the measure of the pressure difference between inlet and outlet regardless of the outlet gas dynamic pressure. The effects of various fuel and oxidant utilizations on the temperature difference are listed in Table 4. The temperature difference in the stack is correlates more with the oxidant utilization than with the fuel utilization. The

Table 3
Effects of fuel, oxidant utilization on pressure difference of 6-kW and 3-kW MCFC stacks (at $i = 100$ mA cm^{-2})[a]

Gas utilization		6-kW			3-kW		
U_f	U_{ox}	$P_{a,in}$	$P_{a,out}$	dP_a	$P_{a,in}$	$P_{a,out}$	dP_a
40	40	130	80	50	160	75	85
50	40	–	–	–	135	70	65
60	40	80	40	40	120	65	55
70	40	–	–	–	110	65	45
80	40	70	35	35	95	60	35
U_f	U_{ox}	$P_{c,in}$	$P_{c,out}$	dP_c	$P_{c,in}$	$P_{c,out}$	dP_c
40	30	–	–	–	240	65	175
40	40	160	70	90	165	30	135
40	50	–	–	–	120	10	110
40	60	80	30	50	85	0	85
40	70	70	30	40	–	–	–

[a] U_f (%), U_{ox} (%), P_a (mm H_2O), P_c (mm H_2O).

oxidant flow, determined by the utilization and current load was used as coolant in the externally-reforming MCFC stack [15]. The effect of gas utilization on the temperature difference in the stack was small compared with the effect current load. The temperature difference in the stack was proportional to utilization, which showed positive values in the static gain matrix (Eq. (17)). The steady-state gain matrix of a 6-kW MCFC stack can be expressed as follows:

$$K = \begin{pmatrix} 1.000 & 0.027 & 0.054 \\ 0.714 & -1.000 & 0.000 \\ -0.308 & 0.000 & -0.692 \end{pmatrix} \quad (17)$$

The K_{23} and K_{32} values indicate that there is no interaction between the anode (cathode) pressure drop and the oxidant (fuel) utilization in the absence of gas cross-over. Each element in the static gain matrix was calculated as a partial derivative that was evaluated with all of the manipulated variables except the relevant manipulated variable held constant. The negative static gain shows the relation in each operating variable is inversely proportional. From the static

Table 4
Effects of various fuel and oxidant utilization on temperature difference of 6-kW and 3-kW MCFC stacks (at $i = 100$ mA cm^{-2})

Gas utilization		6-kW			3-kW		
U_f (%)	U_{ox} (%)	T_{out} (°C)	T_{in} (°C)	dT	T_{out}	T_{in}	dT
40	40	676.2	587.1	89.1	677.2	578.5	98.7
50	40	–	–	–	678.1	578.1	100.0
60	40	676.7	586.4	90.3	677.1	576.4	100.7
70	40	–	–	–	678.8	577.2	101.6
80	40	678.3	587.1	91.2	–	–	–
40	40	676.2	587.1	89.1	677.2	578.5	98.7
40	50	–	–	–	678.2	577.2	101.0
40	60	680.6	589.6	91.0	681.1	575.4	105.7
40	70	683.7	590.5	93.2	–	–	–

gain matrix, all the relative gains were calculated in the following RGA [12]:

$$\Lambda = \begin{pmatrix} 1.0047 & 0.0194 & -0.0241 \\ 0.0194 & 0.9806 & 0.000 \\ -0.0241 & 0.000 & 1.0241 \end{pmatrix} \quad (18)$$

The RGA can be used to provide a measure of the process interactions. This matrix is symmetric and the sum of the elements is unity for each row and for each column. The large diagonal elements in Eq. (18) show the strong correlation between relative controlled and manipulated variables. The first row of the above RGA (Λ) shows relevant effects of manipulated variables on the temperature difference. The relatively small values of second and third elements (λ_{21}, λ_{31}) in the first column in the RGA indicate that the pressure drops are little affected by the electrochemical reaction (Eqs. (1) and (2)). In the above RGA matrix, the diagonal elements are predominant and this indicates a proper control strategy including a process interactions and proper pairing between the controlled and the manipulated variables. The negative relative gains in Eq. (18) show that the opening or closing input has a serious and undesirable effect on the relevant output [12]. It follows that y_3 should not be paired with u_1, and y_1 should not be paired with u_3. In other words, the temperature difference should be controlled by current density, and the pressure drops of the anode and the cathode should be controlled by the fuel and the oxidant utilization, respectively [17–19]. The above recommendation about pairing is based solely on steady-state information. Process dynamics should also be considered, however, in choosing a controller pairing. The singular values of the above matrix are 0.5873, 0.8098, and 1.4439. The condition number of this system is 2.4501, which is the lowest value for all possible configurations between controlled and manipulated variables. This condition number shows that the transfer function matrix is well-conditioned [12]. The small condition number shows that the pairing between manipulated and controlled variables is well-selected and the system can be easily controlled.

4.1.2. The 3-kW MCFC system

The influence of current load on the stack inlet and outlet temperature measured during the operation in a 3-kW MCFC stack is given in Fig. 6. The outlet temperature of the stack increases linearly as the current load is increased, as in the case of the 6-kW stack. Unlike the 6-kW stack, however, it is possible to maintain the inlet temperature of the 3-kW stack at around 580°C, because the outlet temperature is less than the limited range at the higher load current density (150 mA cm^{-2}). This explains why the temperature difference in the stack depends not only on the current load but also on the cell size, which determines the amount of heat released from the stack by the exothermic electrochemical reaction, as already explained. The other effects on the temperature distribution within the safety limit

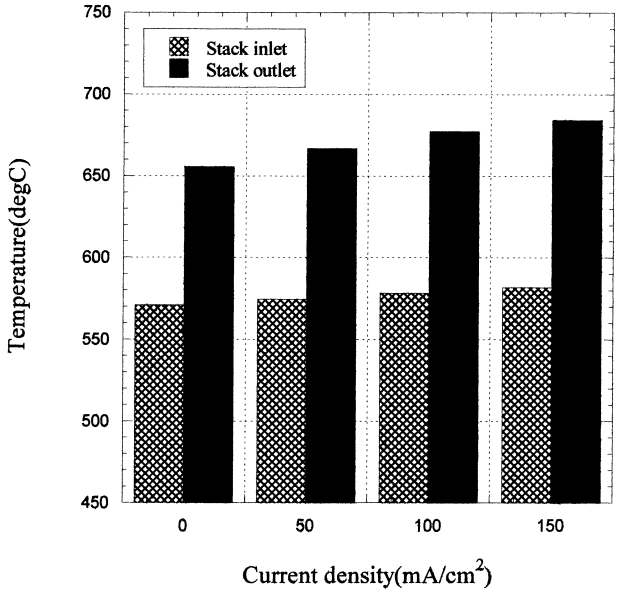

Fig. 6. Effects of current load on temperature at inlet and outlet measured in 3-kW MCFC stack at $U_f/U_{ox} = 40/40\%$.

at full load are the lower pressure drops which occur in the stack, as shown in Fig. 7. The increase of stack outlet temperature is linearly proportional to that of current density. As in the 6-kW stack, a slight increase in inlet temperature also occurs in the 3-kW stack due to the heat released in the stack under current load.

The effects of current load on the pressure drop in the 3-kW stack at the anode and the cathode inlets is presented in Fig. 7. The decreasing rate of pressure difference between the anode and the cathode with current load is smaller than that of a 6-kW stack, which is influenced by the small size and the soft-rail type separators used in this stack. The effects of fuel and oxidant utilization on the pressure difference in

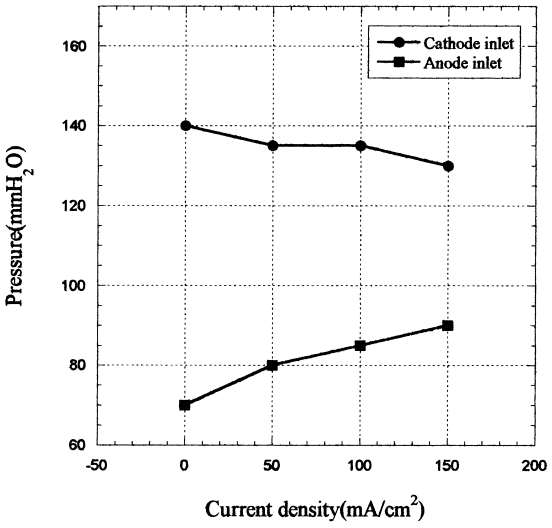

Fig. 7. Effects of current load on anode and cathode inlet pressure measured in 3-kW MCFC stack at $U_f/U_{ox} = 40/40\%$.

the 3-kW stack are also listed in Table 3. As in the 6-kW MCFC stack, the pressure drop at the anode and the cathode appears to be inversely proportional to the utilization rate. Based on the steady-state data, the steady-state gain matrix of the 3-kW MCFC stack can be shown as

$$K = \begin{pmatrix} 1.000 & 0.409 & 0.642 \\ 0.571 & -0.929 & 0.000 \\ -2.58 & 0.000 & -1.000 \end{pmatrix} \quad (19)$$

Compared with the 6-kW MCFC stack, the influence of the fuel and the oxidant utilization rates as the temperature difference is more severe (K_{12}, K_{13}). This explains why the cooling effect of fuel and oxidant flow increases due to the small heat capacity of the 3-kW stack which is composed of five unit cells. From the static gain matrix, the RGA of the 3-kW stack can also be calculated easily as follows:

$$\Lambda = \begin{pmatrix} 0.9208 & 0.2318 & -0.1526 \\ 0.2318 & 0.7682 & 0.000 \\ -0.1526 & 0.000 & 1.1526 \end{pmatrix} \quad (20)$$

Similar to that observed for the 6-kW stack, the dominant diagonal elements in the static gain matrix show proper pairing between the operating variables. The oxidant utilization and temperature difference in the stack could not be paired on account of the negative relative gain (λ_{13}). The current density and cathode pressure drop in the stack could not be paired on account of the negative static gain (λ_{31}). The singular values of this system are 0.6220, 1.0662, and 1.5202. The condition number of this system is 2.4433, which is a little higher than that for the 6-kW stack. These condition numbers of the two MCFC stacks are <2.5 and, therefore, show that the variables for the two kW-scale MCFC stacks are properly selected and well-paired [12].

4.2. Dynamic characteristics of kW-scale MCFC systems

4.2.1. The 6-kW MCFC system

The dynamic characteristics of the kW-scale MCFC stack can be evaluated from the response of the unit step test. The time constant in a first-order plus time delay model is the time when the corresponding controlled variables reach 63.2% of steady-state gain, applying the unit-step change of respective manipulated variable to the system (Fig. 3). For kW-scale stacks, all the responses of controlled variables according to the step change of manipulated variables were shown immediately without a time delay. The response of the temperature difference in the stack to the manipulated variables was the order of a few hours, while the response of the pressure drops was a few seconds. Obtaining the time constants of the temperature difference (τ_{11}, τ_{12}, τ_{13}) was time-consuming, because it took several hours to reach the steady-state condition. The average time constants from several different operating regions were used due to the time varying characteristics and performance decay of the stack.

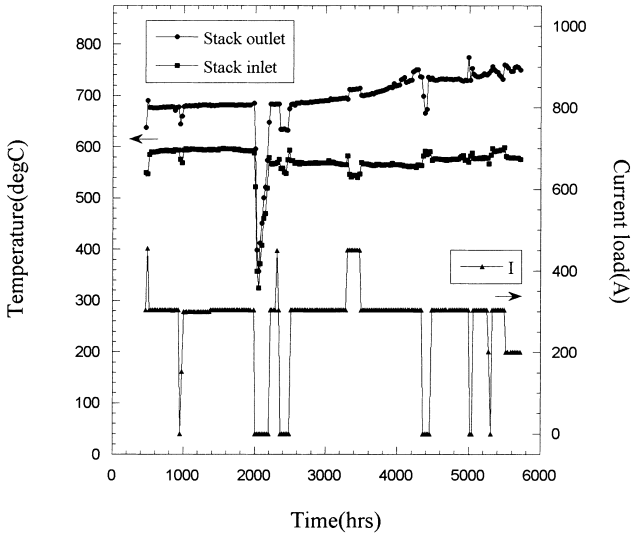

Fig. 8. Variation of temperature at stack inlet and outlet and current load of 6-kW MCFC stack during continuous operation.

Fig. 8 shows the variation of current load and the inlet and outlet temperatures of the 6-kW stack during the 5760 h of operation (including 445 h of pretreatment). For the first 2000 h, the temperature difference in the stack did not vary with the current load and fuel and oxidant utilization. The temperature difference between the stack inlet and outlet increased with operating time regardless of the application of load after thermal cycling for about 2000 h. From an operation test at a higher load current density, namely, 150 mA cm^{-2} for 3300 h, the stack performance degradation was accelerated due to a more severe temperature distribution, as shown in Fig. 4. After this, the temperatures of the upper unit cells increased abnormally, which indicated the formation of a hot spot due to gas cross-over [4]. A larger temperature difference developed at current density of 100 mA cm^{-2} after ~4300 h of operation. These time-varying dynamic characteristics of the system makes it necessary to update the model with operating time and makes it difficult to construct a simulation model applicable to any situation. The simple unit step test used here can be easily adopted to update the dynamic model for long-term operation.

Four sampling regions were selected to analyze the dynamic characteristics of the 6-kW MCFC system, as shown in Table 5. Each region has some variations in fuel and oxidant utilization and current load, used to calculate the time constants representing the response of paired variables. To compare the dynamics at different operating regions, regions 1 and 3 are enlarged in Figs. 9 and 10, respectively. Two different operating ranges in region 1 were used to analyze the system dynamics from the various changes in the current load and the fuel flow rate. First, the effects of current load on the temperature difference without changing the fuel flow rate were measured between 444 and 449 h of operation (see Fig. 9). Both the inlet and the outlet temperature decreases with increase in fuel and oxidant flow

Table 5
Change of manipulated variables (fuel, oxidant utilization and current load) of the 6-kW MCFC stack with operating time

Test region	Operating time (h)	Gas utilization (%)		Current load (A)
		Anode	Cathode	
1	440–510	0–40	0–40	OCV → 150 → 300 → 450 → 300
2	945–960	40	40–60	300 → OCV → 300
3	2300–2550	40–60	40–60	300 → 450 → OCV → 300
4	3300–3500	40–60	40	300 → 450 → 300

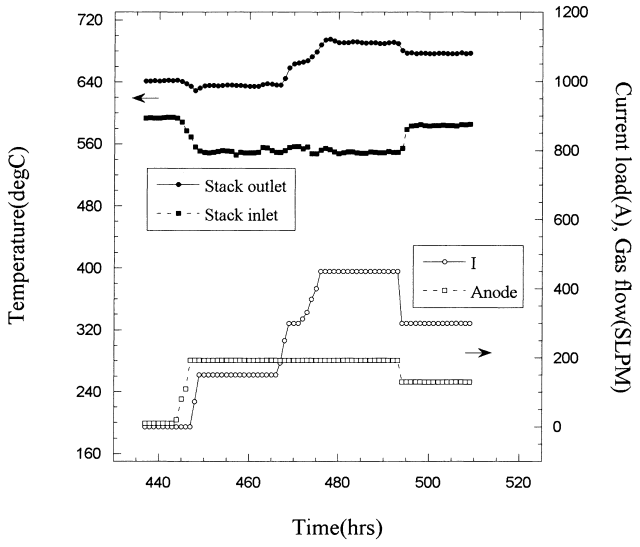

Fig. 9. Effects of current load and anode flow rate on temperatures at inlet and outlet of 6-kW MCFC stack between 430 and 510 h of operation.

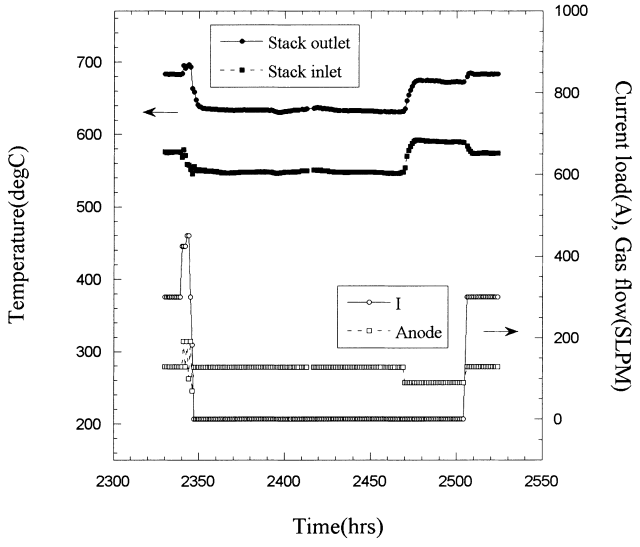

Fig. 10. Effects of current load and anode flow rate on temperature at inlet and outlet of 6-kW MCFC stack between 2330 and 2530 h of operation.

rates in this region. The inlet temperature difference (43°C) is influenced more by the flow rate than by the outlet (6.7°C). The stack inlet temperature is affected mainly by the flow rate supplied to the stack than the outlet. Notice that the outlet temperature in region 1 is proportional to that of the current load, but the inlet temperature is inversely proportional to that of the fuel flow rate. Second, between 467 and 476 h, the current load was changed from 150 to 450 A without any change to the fuel flow (see Fig. 9). The current load affected the stack outlet temperature proportionally which also applied to the region around 493 h. The temperature difference decreased from 142.4 to 92.9°C as the current load and fuel gas flow decreased.

Fig. 10 shows the effects of current load and fuel flow rate on the temperature of stack at the inlet and the outlet for region 3 in Table 5. Between 2340 and 2347 h, the inlet and outlet temperatures decreased when the current load was changed from 300 to 0 A. The decrease in the outlet temperature (50°C) is greater than that of the inlet (27°C), as already explained. In the region between 2470 and 2506 h of operation, the fuel utilization was increased from 40 to 70% without changing current load. This caused all the temperatures in the stack to increase by about 40°C. In the region between 2506 and 2524 h of operation, the stack outlet temperature was increased by increasing the current load while stack inlet temperature was decreased by increasing the fuel flow. After thermal cycling, the dynamic characteristics were changed by some temperature rises in the stack compared with region 1.

The dynamic test in region 2 was used mainly to determine the time constant (τ_{11}) related to change in current load with constant oxidant and fuel utilization. It was obtained by a unit step change of current load, 300 A, for 15 h. The fuel utilization was changed from 40 to 60% to get the temperature change at the OCV for only 1 h at around 950 h of operation. In the region 4, the stack operated at a higher current load for about 200 h, which made the temperature difference in the stack over 140°C. In this region, the severe operating condition was set to test the performance of the stack and the effect of fuel utilization.

The response of the pressure difference to the change in manipulated variables is much faster than that of the temperature difference, as already mentioned. The effects of fuel (oxidant) utilization on the pressure drop of the anode (or

cathode) is so fast that the time constant could be set to 1 s, equal to the sampling time in the 6-kW stack. Without gas cross-over, the effects of fuel utilization on the anode pressure drop could be eliminated and so could the effects of oxidant on the cathode. The effect on the pressure drop by step change in the current load was shown immediately and the electrochemical reaction reached the steady-state after 8 s which is required for a stack composed of unit cells with large area electrode (Eqs. (1) and (2)). Based on the experimental data, the transfer function of the 6-kW MCFC stack representing the relationship between manipulated and controlled variables in a Laplace transform is as follows:

$$\begin{pmatrix} \mathrm{d}T \\ \mathrm{d}P_\mathrm{a} \\ \mathrm{d}P_\mathrm{c} \end{pmatrix} = \begin{pmatrix} \dfrac{1.000}{9102s+1} & \dfrac{0.027}{12547s+1} & \dfrac{0.0541}{13653s+1} \\ \dfrac{0.714}{5s+1} & \dfrac{-1.000}{s+1} & 0.000 \\ \dfrac{-0.308}{5s+1} & 0.000 & \dfrac{-0.692}{s+1} \end{pmatrix} \times \begin{pmatrix} i \\ U_\mathrm{f} \\ U_\mathrm{ox} \end{pmatrix} \quad (21)$$

4.2.2. The 3-kW MCFC system

Fig. 11 shows the time-dependent effects of a step-change in current load on the temperature difference between the inlet and the outlet of the stack to measure the time constants at various current loads. The response in Fig. 11 showed the typical behavior of the first-order transfer function without time delay as the current load decreased from 900 A to three lower current loads, namely, 600, 300, 0 A. The temperature difference in the 3-kW stack at the highest current load (900 A) was 102.3°C, which decreased proportionally to the change in current load. When the current load was lowered from 900 to 0 A, the temperature difference in the stack was 84.4°C. After a step change in the current load was applied for about 1150 min, the response showed the inverse response as in the case of load-up. The response showed higher order dynamics as the current load increased especially from 0 or 300 to 900 A, but this could be considered the first-order transfer function [12]. The effect of fuel (oxidant) utilization on the pressure drop of the anode (or cathode) is also equal to the sampling time. Without gas cross-over, the effects of fuel utilization on the anode pressure drop is negligible, and so is oxidant utilization on the cathode pressure drop. The effect on the pressure drop of a step change in current load was shown immediately without time delay and the electrochemical reaction reached a steady-state condition after 3 s, which is due to the smaller number of unit cells. As with the 6-kW system, the transfer function of the 3-kW system was also established on the basis of the above experimental data. The transfer function of the 3-kW MCFC stack is given by

$$\begin{pmatrix} \mathrm{d}T \\ \mathrm{d}P_\mathrm{a} \\ \mathrm{d}P_\mathrm{c} \end{pmatrix} = \begin{pmatrix} \dfrac{1.000}{11378s+1} & \dfrac{0.409}{10012s+1} & \dfrac{0.642}{10240s+1} \\ \dfrac{0.571}{2s+1} & \dfrac{-0.929}{s+1} & 0.000 \\ \dfrac{-0.258}{2s+1} & 0.000 & \dfrac{-1.000}{s+1} \end{pmatrix} \times \begin{pmatrix} i \\ U_\mathrm{f} \\ U_\mathrm{ox} \end{pmatrix} \quad (22)$$

All the static gains used in the transfer function model (Eqs. (21) and (22)) were from the already evaluated values in the steady-state gain matrix (Eqs. (17) and (19)). The larger time constants in the first row of the transfer function matrix show that the response of temperature difference is the order of a few hours. The smaller time constant in the above transfer function signifies a quick response. The time constant (9102) in the first element of the transfer function matrix in Eq. (21) is smaller than that in Eq. (22) because the 6-kW stack (20-cell) produces more heat than the 3-kW stack (5-cell) under load. The static gains and time constants in the above transfer function could be changed with operation time due to time-dependent characteristics of the MCFC stacks, as already explained. The transfer function in Eq. (21) was evaluated from the experimental data, which were collected between 1000 and 2000 h. Fig. 12 shows the change in dynamic characteristic of the pressure drops, as operating time elapses. After thermal cycling for around 2000 h, the pressure difference between the anode and the cathode increased on account of the increasing pressure drop at each electrode, as shown in Fig. 12. The rise in the pressure drop at each electrode is due to an increase in polarization by micro-structure changes in the porous components, loss and redistribution of electrolyte, etc. [4].

With the dynamic model evaluated here, all the available advanced control technologies can be used to control easily

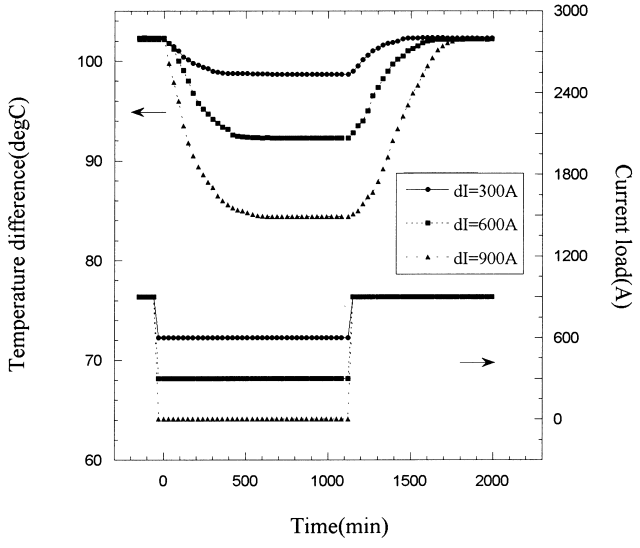

Fig. 11. Effects of various current load change on temperature at inlet and outlet of 3-kW MCFC stack $U_\mathrm{f}/U_\mathrm{ox} = 40/40\%$ (d*I*: current load change).

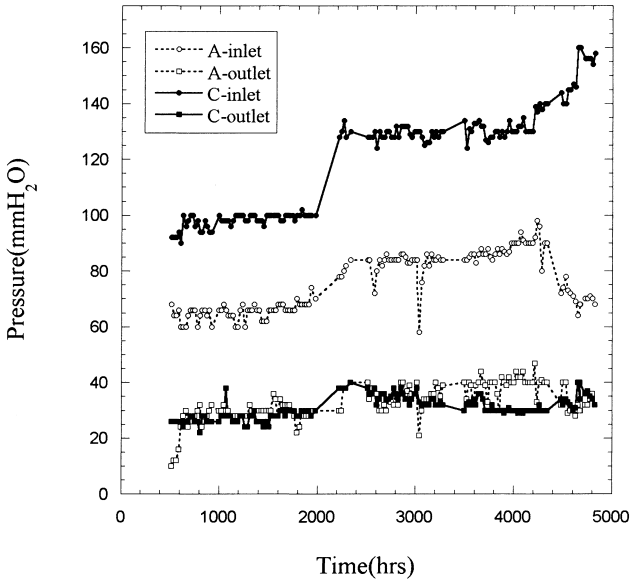

Fig. 12. Variation of pressure drops of anode and cathode of 6-kW MCFC stack during continuous operation (A: anode; C: cathode).

the above MIMO system (Eqs. (21) and (22)) [18–20]. The uncertainties between the process and simulation models can be solved by the unit step test periodically or by adaptive control based on on-line model update. There are also techniques for the design of true multi-variable controllers which utilize all available process outputs jointly to make decisions on all inputs. Such techniques as optimal control (LQ), dynamic matrix control (DMC), and internal model control (IMC) can be used to eliminate the interactions and provide optimal control [21].

5. Summary and conclusion

Dynamic models of kW-scale MCFC stacks has been developed on the basis of experimental data. The controlled variables, which should be controlled within the safety range to ensure high performance and reliable operation of the stack, are the temperature difference in the stack and the anode and the cathode pressure drops. Three manipulated variables, namely, current load, fuel and oxidant utilization are selected to control the three controlled variables. The two dynamic models are MIMO systems with three inputs and outputs, respectively. These models are represented as transfer function matrices and show the dynamic relationship between the manipulated and controlled variables expressed in normalized deviation forms. Each element in the dynamic models is a first-order transfer function with the assumption that the higher over-damped model can be represented as first-order without loss of generality. The non-zero, off-diagonal elements in the transfer function matrix show some interactions between operating variables, and zero elements show no interaction between fuel and oxidant flow without gas cross-over. The unit step change of each manipulated variable to the respective controlled variable is used to acquire the steady-state gain and the time constant. The stability of both dynamic models is analyzed using the RGA method, which is used to calculate the relative gain based on static gains in the transfer function. The large diagonal elements in the RGA matrix show that the pairing between manipulated and controlled variables is well-determined. Proper pairing is also confirmed by the SVA method with smaller condition numbers in each system.

Acknowledgements

This work was supported by Korea Electric Power Corporation and R&D Management Center for Energy and Resources of The Korea Energy Management Corporation.

References

[1] L.J.M. J. Blomen, M.N. Mugerwa (Eds.), Fuel Cell Systems, Plenum Press, New York, 1993.
[2] H. Yasue, H. Kato, K. Takasu, J. Power Sources 71 (1998) 89–94.
[3] P.H. Eichenberger, J. Power Sources 71 (1998) 95–99.
[4] S.A. Hong, T.H. Lim, S.W. Nam, I.H. Oh, H.C. Lim, Korean J. Chem. Eng. 17 (2000) 193–197.
[5] T.L. Wolf, G. Wilemski, J. Electrochem. Soc. 130 (1983) 48–55.
[6] M. Yamaguchi, T. Saito, M. Izumitani, S. Sugita, Y. Tsutsmi, IEEE Trans. Ind. Electron. 37 (1990) 378–386.
[7] W. He, Int. J. Energy Res. 23 (1999) 1331–1344.
[8] W. He, Energy Convers. Manage. 39 (1998) 775–783.
[9] W. He, Q. Chen, Proc. ASME 37 (1997) 249–256.
[10] M.D. Lukas, K.Y. Lee, H.G. Ayagh, IEEE Trans. Energy Convers. 14 (1999) 1651–1657.
[11] D.J. Hall, R.G. Colclaser, IEEE Trans. Energy Convers. 14 (1999) 749–753.
[12] D. Seborg, T.F. Edgar, D.A. Mellichamp, Process Dynamics and Control, Wiley, New York, 1989.
[13] W. He, Q. Chen, J. Power Sources 55 (1998) 182–192.
[14] B. Bosio, P. Costamagna, F. Parodi, Chem. Eng. Sci. 54 (1999) 2907–2916.
[15] J.-H. Koh, B.S. Kang, H.C. Lim, J. Power Sources 91 (2000) 161–171.
[16] J.-H. Koh, B.S. Kang, Accepted by Int. J. Energy Res.
[17] P. Grosdidier, M. Morari, B.R. Holt, Ind. Eng. Chem. Fundam. 24 (1985) 221–235.
[18] D.S. Hwang, P.L. Hsu, Ind. Eng. Chem. Res. 36 (1997) 2739–2748.
[19] S.H. Hwang, Ind. Eng. Chem. Res. 34 (1995) 225–236.
[20] A.P. Loh, C.C. Hang, C.K. Quek, V.U. Vasnani, Ind. Eng. Chem. Res. 32 (1993) 1102–1107.
[21] S.J. Shiu, S.H. Hwang, Ind. Eng. Chem. Res. 37 (1998) 107–119.